ACTA ACUSTICA UNITED WITH ACUSTICA
Vol. 90 (2004) 62 – 69

Feasibility of B-Scan Imaging in Sediment by Means of Parametric Transmission Technique

Jacques Marchal, Pierre Cervenka
Laboratoire de Mécanique Physique associé au CNRS (UMR 7068), Université Pierre et Marie Curie,
2, place de la gare de ceinture, F-78210 Saint-Cyr-l'Ecole

Summary
The feasibility to perform B-scan imaging of buried objects in sediment by means of a parametric transmitter is investigated. The theoretical bases upon which the system is modeled are described. Numerical simulations are performed to estimate the expected lateral resolutions and the available acoustic levels. The influence of the main parameters is analyzed: diameter and altitude of the projector, primary frequencies and frequency ratio of primary-to-secondary fields. The optimal configurations are searched. A comparison with equivalent linear systems is presented.

PACS no. 43.25.Lj, 43.30.Lz

1. Introduction

Several underwater activities require to detect and to track buried pipes in sediments. Magnetometers are routinely used for this task. In some instances, additional information is also needed: What is the size of the pipe? At what depth is it buried? The answer to these questions can be searched by means of acoustical imaging [1, 2]. The simplest method consists in using the B-scan type imagery with a vertical beam: the image is built line by line, each line being acquired with a single ping. The quality of the resulting image depends mainly on the lateral resolution of the transmitted beam, and on the available acoustic level. The feasibility of using a parametric transmitter for this type of application is investigated here. Such a technique is known to produce high resolution, low frequency beams with a small transducer. Many authors addressed the penetration of parametric beams in sediments, for geological applications or object detection [3, 4, 5, 6, 7, 8, 9]. In the present paper, the expected performances are de- lineated by scanning several parameters of the parametric transmitter within a numerical model that has been specifically tailored to treat the problem in a particular geometry. The targeted lateral resolution is about 20 cm in the first meter under the interface water / sediment. Although the original issue concerned imaging pipes, the presented study is indeed also relevant for other types of buried objects at similar depths.

The paper is organized as follow: The modeled system is first described. The theoretical bases upon which the numerical model is built are next recalled. Effects of the projector parameters, and of the geometry of the system are then studied by means of simulations. Finally, a comparison with a linear based system is presented in the conclusion.

Received 28 June 2002,
accepted 6 October 2003.

2. Modeled System

The modeled imaging system is based on the B-scan technique, i.e. the images are built by concatenation of adjacent lines. Each line corresponds to a vertical sector scanned by a single acoustic beam. The information is derived from the temporal evolution of the backscattered echoes, without any particular beamforming process. Hence, an elementary transmitter consists of a single projector located above the interface water/sediment (Figure 1). The receiving probe can be located either at the same altitude as the projector, or closer to the interface.

The depth of interest in the sediment (denoted d) is smaller than 1 m. The altitude of the transmitter above the interface (denoted h) is between 1 m and 3 m. The altitude restricts the maximal depth of exploration in the sediment. Beyond this value ($d > h$), multiple bounces of the transmitted wave between the antenna and the bottom in the water column interfere with the returned echoes. The altitude of the receiving probe is denoted h'.

One looks at the beamwidth and at the acoustical level of the transmitted beam in the sediment layer. These values depend on many parameters: physical properties of the media, geometry of the system, and characteristics of the transmitted signals. However, the feasibility of the system can be studied by imposing a few characteristic parameters to represent the typical situations that occur in actual pipe tracking.

The antenna is a disk whose diameter D is between 3 cm and 15 cm.

Table I. Modeled acoustic properties of the media.

	Density	Sound speed	Attenuation
Sea water	$\rho_0 = 1026\,\mathrm{kg/m^3}$	$c_0 = 1500\,\mathrm{m/s}$	François-Garrison model
Sediment	$\rho_s = 1860\,\mathrm{kg/m^3}$	$c_s = 1700\,\mathrm{m/s}$	$a_s = 0.4\,\mathrm{dB/m/kHz}$

The simulations are built with a constant acoustic velocity of the active face of the antenna. The chosen value is equivalent to a pressure peak amplitude of 10^5 Pa for each primary wave, i.e. $P_0 = 217\,\mathrm{dB}$ ref. $1\,\mu$Pa rms. This level is realistic in term of technology, and consistent in term of generation of a significant parametric radiation. Note that source levels are classically expressed at a nominal distance of 1 m. It relates to the surface pressure through $SL = P_0 + 20\log(S/\lambda)$, where S denotes the surface of the active face, and λ is the wavelength.

The acoustical properties of the modeled media are given in Table I. The sediment is modeled as a fine sand material that behaves like a homogeneous, absorbing liquid. One assumes that the coefficient of absorption α_s varies linearly with the frequency F_{BF} in the sediment [10] (α_s in dB / m, a_s in dB / m / kHz, and F_{BF} in kHz):

$$\alpha_s = a_s F_{BF}. \tag{1}$$

Note that the modeled interface water / sediment is perfectly plane. Roughness is not taken into account. The micro-relief of actual interfaces may impede the resolution of an imaging system, e.g. because of the off-axis backscatterred echoes. However, a vertical sounding system affords a definite advantage compared to an imaging system that insonifies the interface with a slanted angle. The masking effect of the surface echo for targets located in the vicinity of the interface is drastically reduces: Although the level of the seabed echo may be stronger, the thickness of the hidden layer is limited to the equivalent half pulse length.

3. Theoretical Model

Parametric transmission is obtained by creating two overlapping primary beams at frequencies ω_1 and ω_2. The interaction of these beams generates waves at linear combinations of the primary frequencies. One focuses on the so-called secondary, parametric wave that is created at the difference frequency $\omega_- = \omega_2 - \omega_1$. The main interest of the parametric transmission is the high directivity that can be obtained with an antenna whose size is not very large compared to the wavelength. The other benefits are the large bandwidth potentially available and the low level of the side-lobes in the directivity pattern.

The Westervelt model [11] draws a simple picture of the parametric transmission principle. The primary waves are modeled by collimated beams. They make a source line at the difference frequency that behaves as an end fire array. Such geometry creates a beam pattern whose directivity is proportional to the square root of the array length. In the particular case presented here, the primary waves are strongly attenuated in the sediment so that most of the effective interaction takes place in the water column. The extent of the parametric source is therefore commensurate to the altitude h.

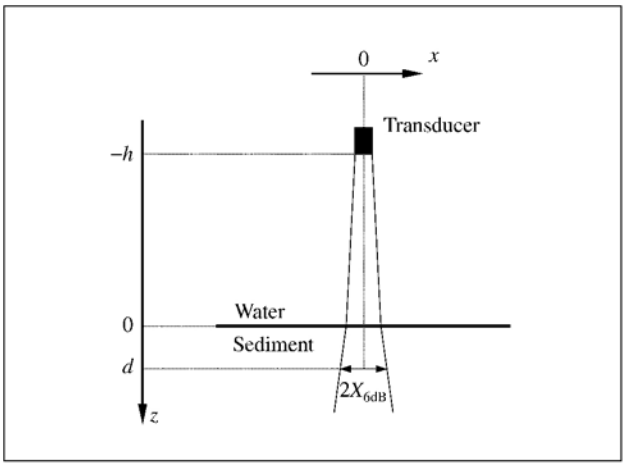

Figure 1. Geometry of the modeled system.

The Westervelt model does not take into account the actual lateral geometry of the primary beams. Moffet and Mellen [12] used a representation of the primary radiation by means of plane waves in the nearfield, and spherical waves in the farfield. The transition between the two zones occurs at the Rayleigh distance R:

$$R = S/\lambda_{HF}. \tag{2}$$

S is the surface of the antenna, and λ_{HF} is the mean primary wavelength. The Rayleigh distance varies from 1.4 cm up to 12 m in this study. It encompasses a large range compared to the altitude h, so that no simplifying assumption can be straightforwardly introduced to model the primary beams.

The saturation phenomenon can impede the efficiency of the parametric conversion. The characteristic length is the shock formation distance:

$$l_s = \frac{\rho_0 c_0^3}{\beta \omega_{HF} P_0}, \tag{3}$$

where ρ_0, c_0, β, ω_{HF} and P_0 are respectively the density, the sound speed, the nonlinear coefficient (3.5 in water), the mean primary angular frequency and the pressure at the surface of the antenna. The shock formation distance varies between 1.6 m and 50 m with the parameters selected in this study. The lower part of this range is at the same order of magnitude as distance h so that us-

ing a model that takes into account saturation is preferable to derive correct estimations. However, saturation effects are not likely to be prominent, so that the influence of the source level is not studied.

The model used to perform the numerical simulations presented here is based on the spatial Fourier formalism in order to handle properly the diffraction phenomenon [13]. Harmonic acoustic fields are broken into plane waves whose distribution of the signature in an observation plane is given by the corresponding spatial 2-D spectra. The initial conditions are given by the primary spectra computed in the reference plane that the active face of the antenna defines.

In the weak nonlinear assumption, one assumes that most of the parametric radiation is created by the only interaction of the primary waves. The primary beams are described as in the linear model, i.e. spectra are derived in any plane parallel to the reference plane through the application of a linear propagation operator. These modes are introduced in the source term of the non-linear second order wave equation. The solution of this equation yields the secondary spectrum.

Saturation is taken into account by altering the primary spectra with a taper function appended to the linear attenuation. The extra-attenuation factors are derived by solving the exact, second order, 1-D non linear equation.

A detailed description of the modeling of the parametric transmission with the spatial Fourier formalism can be found in [14]. The expressions that are implemented in the numerical model are only recalled in the following.

The secondary spectrum is calculated at the water-sediment interface with:

$$A(\boldsymbol{f}_-) = \mathrm{j}\frac{\beta\rho_0\omega_-}{2c_0}\mathrm{e}^{\mathrm{j}k_{z-}h}\iint \mathcal{A}^*(\boldsymbol{f}_1)\mathcal{A}(\boldsymbol{f}_2{=}\boldsymbol{f}_1{+}\boldsymbol{f}_-) \cdot \int_0^h u^*_{1,0}(z)u_{0,1}(z)\exp(-\alpha z + \mathrm{j}\Delta k z)\,\mathrm{d}z\,\mathrm{d}\boldsymbol{f_1}, \quad (4)$$

where $\boldsymbol{f}$ denotes the spatial frequencies.

- $\mathcal{A}(f_{i=1,2}) = D\,J_1(\pi f_i D)/(2f_i)$ is the spatial Fourier transform of the transmitting aperture. Note that all spectra involved in this equation hold the symmetry of revolution, e.g. $\mathcal{A}(\boldsymbol{f}_{i=1,2}) = \mathcal{A}(f_i)$ but also $A(\boldsymbol{f}_-) = A(f_-)$;
- $\alpha = \alpha_1 + \alpha_2 - \alpha_-$ is a linear attenuation coefficient in water, where $\alpha_i = \alpha(\omega_i)$ is given by the François-Garrison model;
- $\Delta k = k_{z2} - k_{z1} - k_{z-}$, with $k_{zi} = \sqrt{\omega_i^2/c_0^2 - 4\pi^2 f_i^2}$ is the phase gap that exists between the primary source and the created waves;
- The functions $u_{1,0}(z)$, $u_{0,1}(z)$ are the taper functions that account for the extraattenuation of the primary waves. Using the notation $v_i(z) = u_i(z)\exp(-\alpha_i z)$, these functions are computed by solving the differential system:

$$\frac{\mathrm{d}v_{m,n}}{\mathrm{d}z} = -\alpha_{m,n}v_{m,n} + \mathrm{j}\omega_{m,n}\frac{\beta}{2c_0^2} \cdot \left\{\frac{1}{2}\sum_{i+k=m}\sum_{j+l=n} v_{i,j}v_{k,l} - \sum_{i-k=m}\sum_{j-l=n} v_{i,j}v^*_{k,l}\right\}, \quad (5)$$

with the initial conditions $v_{1,0}(0){=}v_{0,1}(0){=}P_0/\rho_0 c_0$, all other values being null $v_{i,j}(0) = 0$.

Because of the large absorption encountered by the primary waves in the sediment, the secondary sources are neglected beyond the interface. Hence, the spectrum given in equation (4) is propagated from the interface to the plane at depth d in the sediment with the linear operator H that accounts for the transmission factor through the interface, plus the loss and linear propagation of the secondary wave in the sediment layer.

$$H(f_-) = T_{w\to s}\exp(-\alpha_s d)\exp(\mathrm{j}k'_{z-}d), \quad (6)$$

with

$$T_{w\to s} = \frac{2\rho_s k_{z-}}{\rho_0 k'_{z-} + \rho_s k_{z-}}, \quad k_{z-} = \sqrt{\frac{\omega_-^2}{c_0^2} - 4\pi^2 f_-^2}$$

and $$k'_{z-} = \sqrt{\frac{\omega_-^2}{c_s^2} - 4\pi^2 f_-^2}.$$

The secondary pressure field in the sediment is finally obtained with the Fourier-Bessel transform:

$$P_{\mathrm{sed}}(z=d,x) = 2\pi\int_0^\infty A(f_-)H(f_-) \cdot J_0(2\pi f_- x)f_-\,\mathrm{d}f_-. \quad (7)$$

4. Analysis of results

For each tested configuration, both the secondary spectrum and diagram are computed according to equations (4) and (7). However for the sake of readability, the analysis is based on the evolution of two values: the -6 dB beamwidth ($2X_{6\mathrm{dB}}$), and the on-axis level.

Because waves undergo a strong attenuation in the sediment, a more rigorous approach would take also into account the radial resolution Δr – dictated by the duration of the transmitted signal – as it alters the actual lateral resolution (Figure 2): A target located off-axis (point A) receives the same acoustic level as another target located on-axis deeper in the sediment (point B). The classical (half) lateral resolution counted at $-x$ dB is expressed through the arc OC, because the acoustic level received at C is x dB lower than at O. However, the attenuation in the sediment over the distance Δr is significant. Hence, the actual (half) width of the resolution cell would be better estimated with the arc OC' such that the difference x dB of received levels is estimated between points C' and B.

Nevertheless, it is more convenient to handle classical lateral resolution. Doing so, the -6 dB lateral resolution gives a more confident estimate than the -3 dB width. For example, an order of magnitude of the attenuation at 50 kHz is 1 dB when $\Delta r = 5$ cm ($\Delta t = 60\,\mu$s). Even if considering a large -2 dB loss in the radial extent of the

resolution cell, the $-6\,\mathrm{dB}$ lateral resolution still describes a realistic effective beamwidth (i.e. at $-4\,\mathrm{dB}$). In addition, the slope of the beam pattern is steeper at $-6\,\mathrm{dB}$ than at $-3\,\mathrm{dB}$ so that the relative effect of attenuation is weaker.

In order to compare various configurations, the displayed levels take into account the two-way interface-target attenuation in the sediment layer:

$$P_{\mathrm{disp}} = 20\log\frac{P_{\mathrm{sed}}(d,0)}{1\,\mu\mathrm{Pa}} - \alpha_s d - 3\,\mathrm{dB}, \qquad (8)$$

(ref. $1\,\mu$Pa rms), where $P_{\mathrm{sed}}(d,0)$ is an estimate of the on-axis pressure amplitude at depth d in the sediment as expressed in equation (7). Note that $P_{\mathrm{sed}}(d,0)$ includes already the one-way attenuation. In order to retrieve the incident pressure level on the target, it is therefore sufficient to compensate the displayed level by adding $\alpha_s d$.

The echo level received at altitude h' is derived by adding to the displayed level (8):

- The target strength I_{TS};
- The coefficient of transmission back through the interface from the sediment to water. On-axis, there is $T_{s\to w} = -3.5\,\mathrm{dB}$;
- The effect of the spherical divergence. Because of the refraction, the equivalent radius is equal to:

$$r = d + h' c_0/c_s. \qquad (9)$$

To summarize, an estimate of the pressure level received by an hydrophone located at the altitude h' above the interface is:

$$P_{\mathrm{echo}} = P_{\mathrm{disp}} + I_{TS} + T_{s\to w} - 20\log r. \qquad (10)$$

Figure 3 displays an example of secondary beam pattern computed for a typical configuration ($D = 7\,\mathrm{cm}$, $LF = 50\,\mathrm{kHz}$, $HF = 500\,\mathrm{kHz}$, $h = 2\,\mathrm{m}$, $d = 50\,\mathrm{cm}$). The characteristic profile of parametric beams can be noticed, i.e. the quasi-linear flanks and the missing side-lobes.

4.1. Projector parameters (diameter, frequencies)

Figures 4 and 5 ($2X_{6\mathrm{dB}}$) gather all the results obtained with the following fixed parameters:
Depth $d = 50\,\mathrm{cm}$,
Altitude of the projector $h = 2\,\mathrm{m}$.
Other parameters are scanned according to:
Diameter $D = 3\,\mathrm{cm}$, $5\,\mathrm{cm}$, $7\,\mathrm{cm}$, $10\,\mathrm{cm}$ and $15\,\mathrm{cm}$,
Difference frequency $LF = 10\,\mathrm{kHz}$ to $100\,\mathrm{kHz}$, pitch $10\,\mathrm{kHz}$,
Mean primary frequency $HF = 30\,\mathrm{kHz}$ up to $1\,\mathrm{MHz}$ (Table II).

In Figures 4 and 5, points linked by a solid line correspond to the ordered, tested primary frequencies, given the diameter and the parametric frequency. In the general case, the rightmost point of a group corresponds to the lowest mean primary frequency. It can be noticed that most groups exhibit an optimal configuration, i.e. a configuration that gives a minimal aperture of the created beam (the level does not vary significantly).

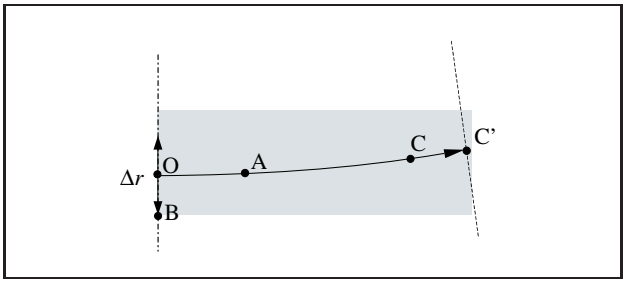

Figure 2. Resolution cell.

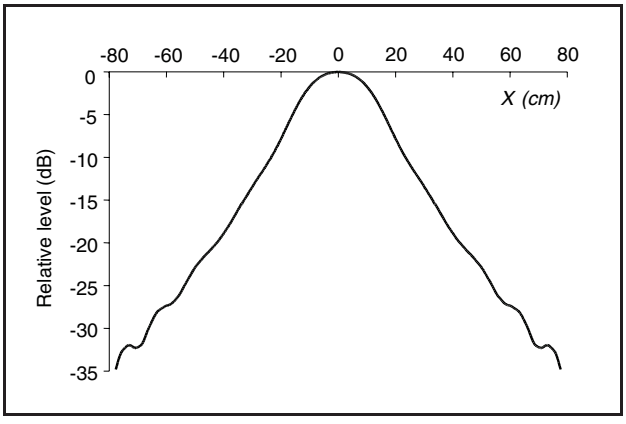

Figure 3. Simulated secondary beam pattern ($D = 7\,\mathrm{cm}$, $LF = 50\,\mathrm{kHz}$, $HF = 500\,\mathrm{kHz}$, $h = 2\,\mathrm{m}$, $d = 50\,\mathrm{cm}$).

Table II. Tested combinations of mean primary (HF, kHz) and secondary frequencies (LF, kHz).

	LF									
HF	10	20	30	40	50	60	70	80	90	100
30	X									
60	X	X								
90	X	X	X							
120	X	X	X	X						
150	X	X	X	X	X					
200	X	X	X	X	X	X	X			
300	X	X	X	X	X	X	X	X	X	X
400	X	X	X	X	X	X	X	X	X	X
…	…	…	…	…	…	…	…	…	…	
1000	X	X	X	X	X	X	X	X	X	X

Let us focus now on optimal configurations. The following points can be observed:

- The level increases with the diameter of the projector (approximately according to $40\log D$). This is a normal behavior because the acoustic velocity of the active face is a constant in all the computed simulations. By the way, it indicates that saturation effects are not yet significant.
- Given the diameter, the efficiency of the parametric conversion increases with the difference frequency. However, the absorption in the sediment increases also with the parametric frequency so that it counterbalances the previous effect. As a consequence, there is a range of parametric frequency that maximizes the

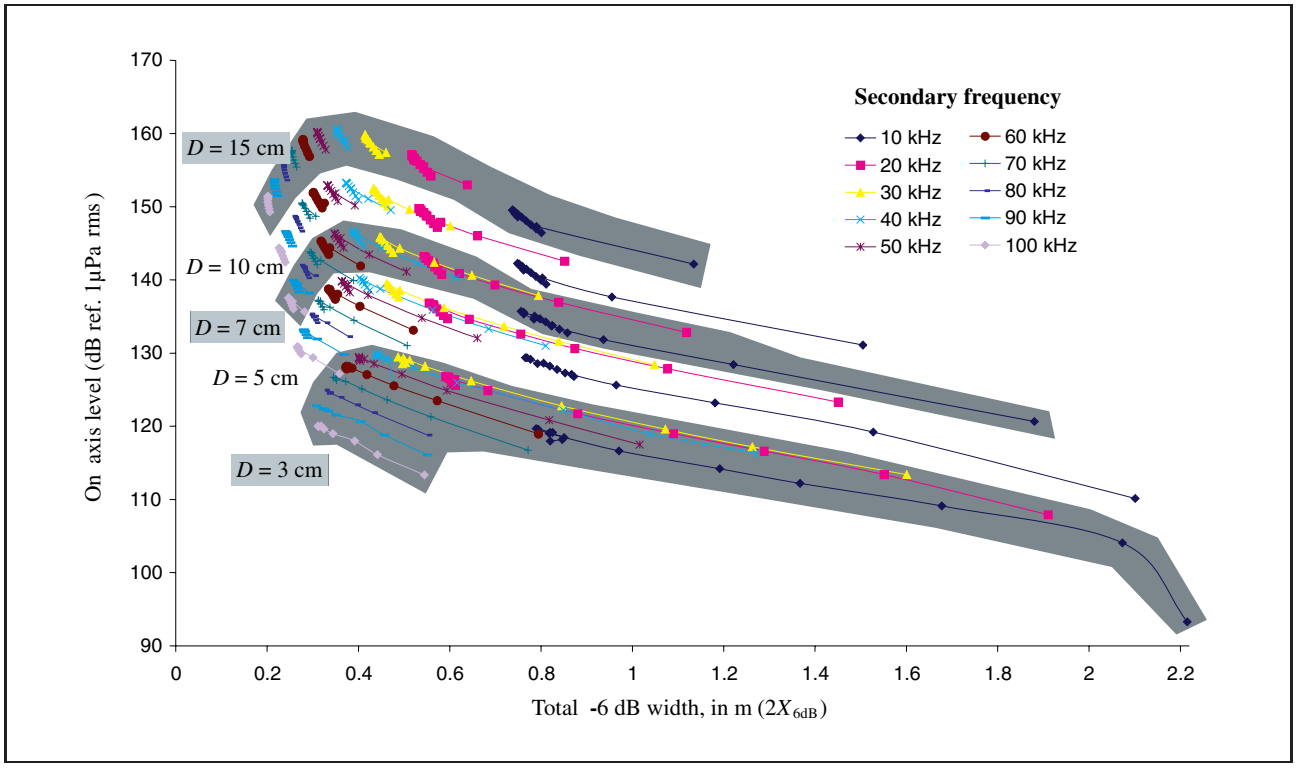

Figure 4. On-axis level $P_{\text{disp}}(d, 0)$ and -6 dB beamwidth at depth $d = 50$ cm (altitude of the transmitter $h = 2$ m).

level. At the tested depth, this range lies between 30 kHz and 60 kHz. This range is shifted toward low frequencies when the depth of the buried target increases.

- The lateral resolution is improved when the parametric frequency is increased.
- Given the parametric frequency, the maximal resolution that can be reached (at the tested depth) is slightly improved when the diameter of the projector increases.
- The primary frequency that enables to reach this best resolution depends on the diameter: The larger the diameter, the lower the optimal primary frequency. Beyond a certain value of the diameter, the theoretical optimal configuration cannot be physical reached. The best resolution is then simply obtained with the lowest primary frequency that the bandwidth of the transducer allows. The minimal frequency ratio of primary-to-secondary fields is then around 3 or 4.

The simulations computed at $d = 50$ cm show finally that the chosen parametric frequency dictates the other parameters leading to an optimal performance, i.e.:

- Minimal frequency ratio (3 or 4);
- Maximal projector diameter. This parameter depends on the primary frequencies and is dictated by technological constraints (accuracy, bulkiness). For example, a reasonable value could be $D \approx 20\lambda_{HF}$.

4.2. Observation in the sediment layer

The previous simulations are performed at a constant depth ($d = 50$ cm). The variations of the beamwidth and of the on-axis acoustic level in the sediment layer are studied here. Frequencies are set to the constant values that correspond to a commercial projector system ($LF = 50$ kHz, $HF = 500$ kHz). It can be noticed that the choice of the secondary frequency at 50 kHz is consistent with respect to the results obtained in the previous section.

4.2.1. Diameter and lateral resolution

The altitude of the projector is still a constant, equal to $h = 2$ m. The following diameters are tested: $D = 3$ cm, 5 cm, 7 cm, 10 cm and 15 cm. Figure 6 displays the evolution of the beamwidth in the layer, from the interface down to 1 m.

The apertures obtained with the smallest diameter ($D = 3$ cm) depart significantly from the otherwise observed patterns, especially close to the interface. In that case, there is a strong diffraction of the primary waves, so that primary as well as secondary beams spread widely.

Whenever the size of the projector is not very small, the conclusion that is drawn at $d = 50$ cm in the previous section is still valid in the complete layer: The lateral resolution is improved when the diameter increases, but the sensitivity of this parameter is weak. Hence, Figures 4 and 5 are representative of the performances that can be expected in the whole sediment layer.

4.2.2. Altitude and lateral resolution

The altitude of the projector varies between 1 m and 3 m in a single configuration: $D = 7$ cm, $LF = 50$ kHz, $HF = 500$ kHz. Beamwidths in the sediment layer (0 m–1 m) are displayed Figure 7. The size of the insonified area at the interface decreases when the projector is closer to

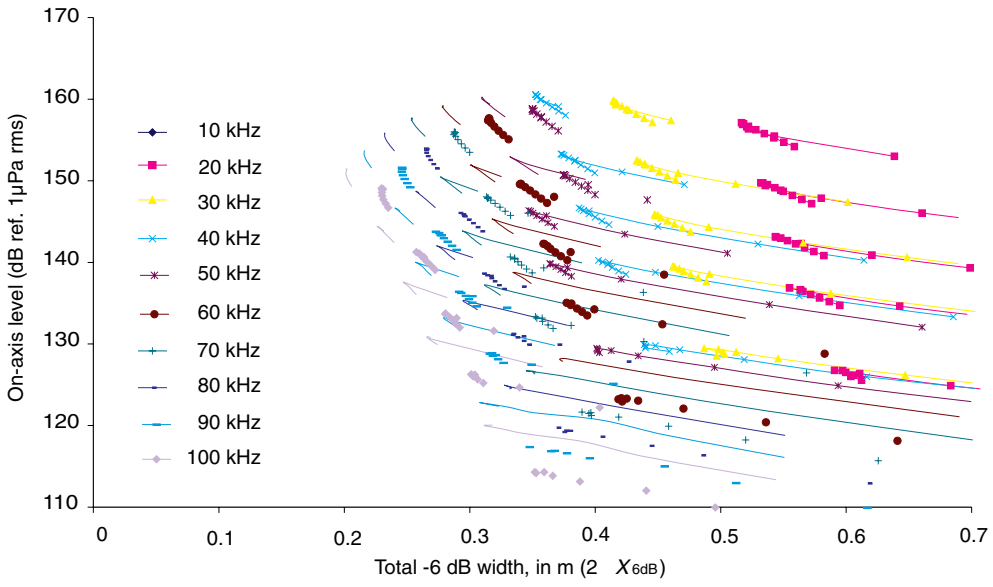

Figure 5.
Zoom of Figure 4.

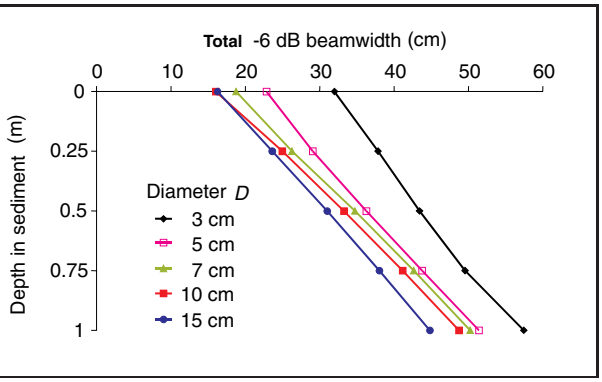

Figure 6. -6 dB beamwidth versus diameter of the projector ($h = 2$ m, $LF = 50$ kHz, $HF = 500$ kHz).

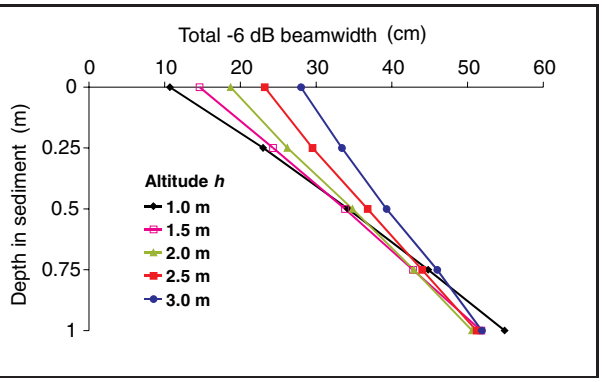

Figure 7. -6 dB resolution versus the altitude of the projector ($D = 7$ cm, $LF = 50$ kHz, $HF = 500$ kHz).

the bottom. Consequently, the secondary beam diverges in the sediment as much as the size of the initial spot is smaller. However, because the thickness of interest under the interface is small, best resolutions are still achieved with the smallest altitude of the projector. Let us recall that whatever is the B-scan imaging system – i.e. linear or parametric – the altitude h of the transmitter must be larger than the maximal depth to be probed in the sediment layer, because of the multiple specular bouncing from the interface.

4.2.3. Acoustic level and maximal detection depth

Because saturation effect is not significant, the generated secondary pressure level varies with the active face acoustic pressure P_0 and the surface S according to $40 \log P_0 + 20 \log S$. On the other hand, the influence of the altitude of the projector, h, cannot be foreseen straightforwardly from theoretical considerations. Figure 8 displays the levels computed with equation (10), but without taking into account the target strength, i.e. $P_{\text{echo}} - I_{TS}$. The receiving hydrophone is assumed to be located at the constant altitude $h' = 1$ m above the interface. The salient result is that the simulated echo level does not depend significantly on the altitude of the transmitter. Let us recall that at the chosen secondary frequency (50 kHz), the two-ways loss caused by linear absorption account for -40 dB when the target is 1 m deep.

Let us define a threshold level Pt that corresponds to the minimal pressure level that can be detected with the acquisition system, i.e. P_{echo} must be larger than P_t. Given the difference in dB $P_t - I_{TS}$, Figure 8 allows to find at once the maximal detection depth that can be achieved with the settings of the model. For example with $P_t - I_{TS} =$ 130 dB ref 1 μPa rms, the maximal depth is about 70 cm and does not depend on the altitude of the projector.

Note that the threshold level P_t can be considered as the sum

$$P_t = (NL - DI) + DT, \tag{11}$$

where NL, DI and DT are respectively the background isotropic noise level, the directivity index of the receiving

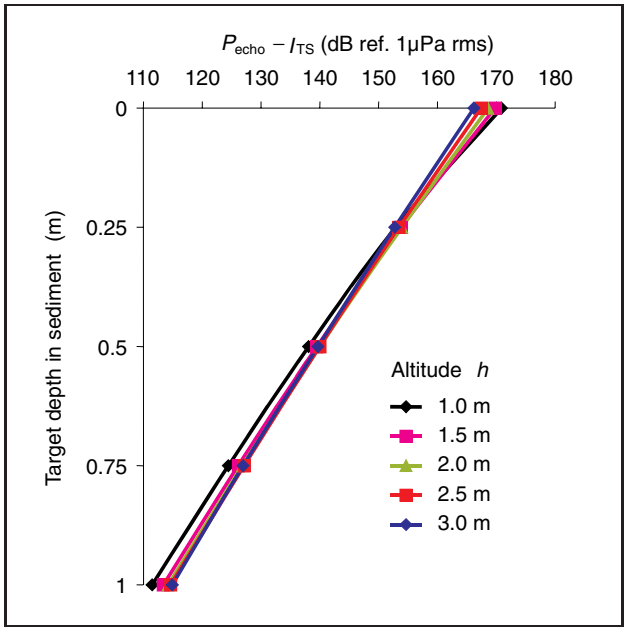

Figure 8. Simulated echo level received at 1 m above the interface without taking into account the target strength. ($D = 7$ cm, $LF = 50$ kHz, $HF = 500$ kHz).

Table III. Parameters of the comparison.

	LF	HF	Diameter D	
Parametric $p = 3$	50 kHz	150 kHz	20 cm	20λ
Linear	50 kHz		30 cm	10λ

probe, and a detection threshold (e.g. 10 dB). The noise level can be estimated with the Wenz model [15]: Considering for example a parametric signal centered around 50 kHz with a bandwidth of 20 kHz, there is $NL < 90$ dB ref 1 μPa rms. Because $DI > 0$, one obtains here the order of magnitude $P_t < 100$ dB ref 1 μPa rms. Within such a noise limited model, an object buried at 1 m depth whose I_{TS} is larger than -10 dB can be detected.

The depth limit (or the minimal target strength) can be improved by increasing the source level. The presented simulations are computed with a surface pressure equal to $P_0 = 10^5$ Pa. With another setting of P_0, the value that must be used to exploit Figure 8 should be corrected according to $P_t - I_{TS} - 40\log(P_0/10^5\,\text{Pa})$.

The reverberation caused by the structure of the sediment is not addressed in this paper. Let us just mention that this phenomenon reduces the contrast of the target echoes. The reverberation level is proportional to the acoustical level and to the 3-D resolution cell. Consequently, an order of magnitude of the expected contrast can be estimated by comparing the reverberation index I_R with the target strength I_{TS}:

$$I_R = I_V + 10\log\left((\Delta x)^2 \Delta z\right), \qquad (12)$$

where I_V is the reverberation index per unit of volume.

In order to keep conservative figures, one consider a maximal beamwidth equal to $\Delta x = 50$ cm in the layer of interest ($d \leq 1$ m). Assuming that the bandwidth is $B = 20$ kHz, the range resolution is $\Delta z = c/2B = 3.8$ cm. Hence the resulting volume of the resolution cell is about 10^{-2} m^3. On the other hand, the order of magnitude of I_V is -30 dB/m^3 [16, 17]. According to equation (12), the reverberation index – about -50 dB – is low compared to the target strength of many objects of interest.

5. Conclusion

Although the parametric conversion exhibits a poor efficiency, the previous simulations show that sufficient acoustic levels can be expected. The main concern is the lateral resolution that can be achieved. Parametric transmission was initially proposed because of the potential high resolution at low frequency. However, optimal solutions are found to be obtained with secondary frequencies around 50 kHz, using as small as possible frequency ratio $p = \omega_{HF}/\omega_{LF}$. This latter parameter is dictated by the available relative frequency bandwidth of the transducer ($1/p$ is required) so that $p = 3$ is a reasonable minimal setting. Note also that the size of the antenna must be as large as possible.

Given these constraints, one may wonder whether a classical, linear system driven directly at the useful frequencies would not produce better performances, still keeping a practical size of the projector. With a linear imaging system, an efficient solution consists in using the same transducer at transmit and at receive: The echographic response is given by the squared transducer directivity pattern. A theoretical drawback of the linear system versus the parametric transmitter is the existence of side lobes. However, their relative level is quite small in the echographic mode: It amounts less than -34 dB with a disk. In addition, the linear system is indeed much more efficient in terms of available acoustic level than the parametric based system.

Table III summarizes the parameters used to perform a comparison between non-linear and linear systems. The useful frequency is equal to 50 kHz. According to the conclusions derived for the parametric projector, the frequency ratio is small ($p = 3$) and the relative diameter of the projector is rather large ($20HF$ wavelengths). The modeled linear projector works directly at 50 kHz. One takes advantage of the benefit afforded by the echographic mode in order to limit the absolute size of the transducer. The comparison is done with half the relative diameter of the parametric projector, i.e. 10 wavelengths. In both cases, the transmitted pressure at the surface of the transducers is $P_0 = 10^5$ Pa. Two locations of the antenna are considered, i.e. $h = 1$ m and 2 m above the interface.

Figure 9 displays the simulated resolutions. They are given with the -6 dB beamwidths for the parametric system. In the linear case, the -3 dB one-way beamwidths are displayed because they are almost equivalent to the -6 dB echographic resolution. The aimed -6 dB aper-

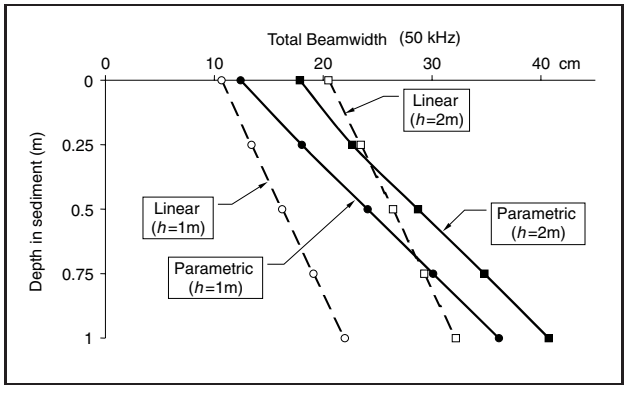

Figure 9. Comparison between resolutions obtained with the non-linear and linear systems.

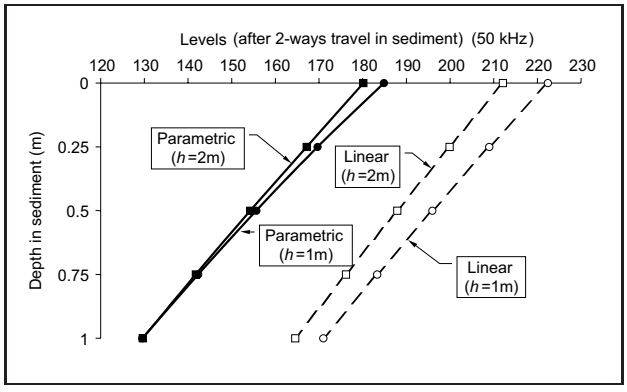

Figure 10. Comparison between levels obtained with the non-linear and linear systems.

ture of 20 cm at 50 cm depth seems out of reach with the parametric system. The echographic response of the linear transducer achieves this requirement up to 1 m depth when located at $h = 1$ m (Note that the -3 dB beamwidth in the nearfield of a transducer can be smaller than the diameter of the active face).

Acoustic levels estimated with equation (10) are displayed in Figure 10. They correspond to the on-axis levels that are received at the altitude of the projector ($h' = h$), taking into account the return attenuation, interface transmission, and spherical spreading losses, and considering a null target strength ($I_{TS} = 0$ dB). The linear solution is much more efficient, with a difference of about 30 dB.

Hence, for imaging properly buried objects such as pipes, the best solution appears to be a classical, linear setup located close to the interface (about 1 m). The angular performance of the parametric system begins barely to compete with the linear system when the altitude increases. But it never fits with the original requirement, i.e. 20 cm lateral resolution. The theoretical benefit afforded by the parametric transmission technique is canceled in this particular application by the very short distance available to build the secondary field.

References

[1] S. Guyonic: Experimental results on detection and classification of buried objects. Underwater Intervention 2001, Tampa, 15-17 January 2001.

[2] S. G. Schock, A. Tellier, J. Wulf, J. Sara, M. Ericksen: Buried object scanning sonar. IEEE J. Ocean. Eng. **26** (2001) 677–689.

[3] T. G. Muir, S. C. V. Horton, L. A. Thompson: The penetration of highly directional acoustic beams into sediments. J. Sound Vib. **64** (1979) 539–551.

[4] J. P. Longuemard, D. Odéro: Etude exp rimentale des conditions de pńtration des ondes acoustiques créés par une antenne paramtrique en fonction des caractères physico-chimiques des sdiments marins. J. Physique **40** (1979) C8/131–137 (supplḿent au no.11).

[5] N. G. Pace, R. V. Ceen: Time domain study of the terminated transient parametric array. J. Acoust. Soc. Am. **73** (1983) 1972–1978.

[6] D. J. Wingham: A theoretical study of the penetration of a water-sediment interface by a parametric array. J. Acoust. Soc. Am. **76** (1984) 1192–1200.

[7] D. J. Wingham, N. G. Pace, R. V. Ceen: An experimental study of the penetration of a water-sediment interface by a parametric array. J. Acoust. Soc. Am. **79** (1986) 363–374.

[8] J. Dybedal: TOPAS: Parametric end-fire array used in offshore application. 13th ISNA, Bergen, 1993.

[9] T. C. Seeberg: A theoretical investigation of the transmission of a phase steered linear and parametric sound beam at a two fluid interface. 13th ISNA, Bergen, 1993, 270–275.

[10] E. L. Hamilton: Geoacoustic modeling of the seafloor. J. Acoust. Soc. Am. **68** (1980) 1313–1340.

[11] P. J. Westervelt: Parametric acoustic array. J. Acoust. Soc. Am. **35** (1963) 535–537.

[12] R. H. Moffet, M. B. Mellen: Model for parametric acoustic sources. J. Acoust. Soc. Am. **61** (1977) 325–337.

[13] J. W. Goodman: Introduction to Fourier optics. McGraw-Hill, New-York, 1968.

[14] P. Cervenka, P. Alais: Fourier formalism for describing non linear self-demodulation of primary narrow ultrasonic beam. J. Acoust. Soc. Am. **88** (1990) 473–481.

[15] G. M. Wenz: Acoustic ambient noise in the ocean: Spectra and sources. J. Acoust. Soc. Am. **34** (1962) 1936–1956.

[16] D. R. Jackson, D. P. Winnebrenner, A. Ishimaru: Application of the composite roughness model to high frequency bottom backscattering. J. Acoust. Soc. Am. **79** (1986) 1410–1422.

[17] L. Guillon: Contribution à l'interprétation géoacoustique de la rétrodiffusion des fonds marins. PhD thesis, Université du Maine, 1999.